Modelling the Physics of Bubble Nucleation in Histotripsy

Matheus O. de Andrade, Seyyed R. Haqshenas, Ki Joo Pahk, Nader Saffari

Abstract— **This work aims to establish a theoretical framework for the modelling of bubble nucleation in histotripsy. A phenomenological version of the classical nucleation theory was parametrised with histotripsy experimental data, fitting a temperature-dependent activity factor that harmonises theoretical predictions and experimental data for bubble nucleation at both high and low temperatures. Simulations of histotripsy pressure and temperature fields are then used in order to understand spatial and temporal properties of bubble nucleation at varying sonication conditions. This modelling framework offers a thermodynamic understanding on the role of the ultrasound frequency, waveforms, peak focal pressures, and duty cycle on patterns of ultrasound-induced bubble nucleation. It was found that at temperatures lower than 50˚C, nucleation rates are more appreciable at very large negative pressures such as -30 MPa. Moreover, for focal peak negative pressures of -15 MPa, characteristic of boiling histotripsy, nucleation rates grow by 20 orders of magnitude in the temperature interval 60 - 100˚C.**

Index Terms— histotripsy, bubble nucleation, classical nucleation theory

I. INTRODUCTION

EARLY investigation of ultrasound-induced bubble activity in biological media aimed to understand and erase the risks of acoustic cavitation in diagnostic ultrasound applications (1). This amounted to a rich body of work addressing fundamental questions such as the effects of pressure and frequency on the likelihood of acoustic cavitation (2), the mechanisms of growth and stabilization of bubbles in biological media (3), and, most importantly, the apparent unpredictability of bubble nucleation in soft tissue (4).

Over the years, an important shift in perspective took place on the role of bubble activity in biomedical ultrasound: cavitation changed from an unwanted side effect to a central mechanism in a range of therapeutic ultrasound applications. As a leading example, ultrasound contrast agents (UCA) demonstrated wide applicability in imaging enhancement, drug and gene delivery applications (5) as well as in opening the blood-brain barrier (6) and increasing ultrasound heating rates for thermal ablation (7). The application considered here, namely histotripsy, harnesses the bioeffects of bubble activity most effectively.

Histotripsy refers to a family of techniques where focused ultrasound is used to noninvasively nucleate and drive the oscillations of bubbles within a volume of soft tissue, leading to the mechanical injury of surrounding areas (8). Histotripsy has been recently shown to be well-tolerated and effective in the mechanical ablation of liver tumours in a phase I trial, the THERESA Study (9).

There are two broad categories of histotripsy, which relate to the mechanism by which bubbles are nucleated (10): boiling histotripsy (11–13) occurs when millisecond-long pulses heat focal tissue to temperatures that are favourable for vapour bubble nucleation and growth (14). Alternatively, intrinsic-threshold histotripsy (15,16) occurs when the focal peak negative ultrasound pressures (17), or nonlinear ultrasound waves reflected from a pre-existing bubble (18), surpass the local tensile strength of the medium, nucleating small, virtually empty, gas pockets (19).

The differing nomenclature might suggest that both are separate phenomena, but there is evidence that they are, in fact, the same phenomena in distinct regimes. Despite the apparent unpredictability of acoustic nucleation in water-like media (4,20), HIFU was shown to repeatably induce bubble nucleation in water, with a strong temperature dependence up to 200 ˚C and qualitative agreement to classical nucleation theory (CNT) (21,22). These experiments were later repeated with an emphasis on histotripsy applications, reporting decreasing pressure threshold magnitudes for increasing medium temperatures (15,23).

Drawing from these results, we build a continuous model of bubble nucleation in histotripsy that can simultaneously account for bubble nucleation at high and low temperatures whilst considering the effects of nonlinear ultrasound pressure fields (14). Previous modelling of spontaneous nucleation in diagnostic ultrasound at constant temperature has found nucleation to be highly dependent on the surface tension of the medium, whilst being additionally dependent on factors such as the ultrasound frequency, sonication time, and targeted volume (1).

Herein, we give an extended theoretical account of the surface tension, analysing how its temperature dependence affects the energetic requirements of nucleation for thermodynamic conditions typical of histotripsy. We build a

de Andrade, Matheus O. is with UCL Mechanical Engineering and the UCL Faculty of Engineering Sciences, University College London, London, United Kingdom (email: m.deandrade@ucl.ac.uk).

Haqshenas, Seyyed R. is with UCL Mechanical Engineering, University College London, London, United Kingdom (email: s.haqshenas@ucl.ac.uk).

Pahk, Ki Joo is with the Biomedical Research Institute, Korea Institute of Science and Technology (KIST), Seoul, Republic of Korea (email: kjpahk@kist.re.kr).

Saffari, Nader is with UCL Mechanical Engineering, University College London, London, United Kingdom (email: n.saffari@ucl.ac.uk).

general model that accounts for the presence of a surface phase between bubble nuclei and the liquid, as well as the possibility of impurities in the medium. An activity factor is then used to modify the surface tension such that its size-dependence in nanoscopic nuclei and potential heterogeneous nucleation can be accounted for in a unified formulation.

The present model draws a relationship between histotripsy focal temperatures and pressure waveforms to the rate at which bubbles nucleate in a steady-state regime. We then integrate this model into simulations of HIFU pressure and temperature fields obtained by solving a Westervelt-type equation and Penne's Bioheat Equation. This modelling framework offers a thermodynamic understanding of the role of the ultrasound frequency, waveforms, peak focal pressures, and duty cycle on patterns of bubble nucleation.

It is then possible to calculate nucleation pressure thresholds as a function of temperature, to map bubble nucleation spatially within the HIFU focus as well as predicting the timescales of bubble nucleation for individual histotripsy protocols at varying sonication parameters. We limit ourselves to nucleation in the absence of pre-existing bubbles, as there are more appropriate ways to model a bubble's response to sonication than the thermodynamic approach developed herein.

II. THERMODYNAMIC MODEL

Phase change, such as the nucleation of bubbles, can only take place in liquids that are either unstable or metastable. Considering an isolated system, thermodynamic equilibrium requires a maximum in entropy $dS|_{U,V,N} \leq 0$ at constant internal energy U, volume V and number of molecules N (24). In unstable systems, phase change happens via spinodal decomposition (25). In metastable systems, the system relaxes towards stability via bubble nucleation. The entropy maximum condition takes place at equilibrium, such that the vapour-liquid equilibrium (VLE) boundary is the lower limit of the stability region in a fluid.

Metastable liquid phases are those where the fluid is stretched below its VLE pressure or superheated above the VLE temperature (26). Under HIFU sonication, metastability might be induced in a liquid momentarily during the tensile part of the ultrasound wave like intrinsic threshold histotripsy, or through nonlinear heat deposition from shock-wave formation as in boiling histotripsy (27). A metastable state is only viable because liquid-vapour phase transitions are delayed by the energetic costs of creating a vapour interface in the bulk of the liquid. This is manifested as a barrier in the system's Gibbs free energy that needs to be overcome before nucleation takes place (28). Assuming an isolated system, the process of bubble nucleation can be seen as the transition between an initial state consisting of a homogeneous liquid, and a final stage consisting of a bubble embryo surrounded by the liquid. The Gibbs free energy G_0 in the initial state, denoted by a subscript 0, is

$$G_0 = U_0 - T_0 S_0 + P_0 V_0 = \mu_l^0 N_l^0, \tag{1}$$

where T denotes temperature, S represents entropy and μ is the chemical potential. The free energy at the final state is

$$\begin{aligned} G &= U - T_0 S + P_0(V_l + V_v) \\ &= P_0(V_l + V_v) - P_l V_l - P_v V_v + \sigma A + \mu_l N_l + \mu_v N_v \\ &\quad + \mu_s N_s \end{aligned} \tag{2}$$

The subscripts l, v and s denote liquid, vapour and surface phases. In this equation A denotes the surface area of bubble nuclei and σ is their surface tension. μ is the chemical potential of the species in question, in either liquid or vapour phases. The chemical potential is a measure of the likelihood of mass transfer or chemical reaction between two chemical species.

By assuming that the chemical composition of the liquid remains constant ($\mu_l^0 = \mu_l$), the free energy of bubble formation $\Delta G = G - G_0$ is given by

$$\begin{aligned} \Delta G &= (P_l - P_v)V_v + \sigma A - (\mu_l - \mu_v)N_v \\ &\quad - (\mu_l - \mu_s)N_s \end{aligned} \tag{3}$$

This expression is derived under the assumption that the initial homogeneous liquid system is much larger than the bubble embryo. The local maximum in the Gibbs Free energy separating metastable and stable phases is then given by $\left(\frac{\partial \Delta G}{\partial V}\right)_{T,P,N} = 0$. This maximum defines the critical point of nucleation (28).

In the timescales at which histotripsy bubble nucleation takes place, it is possible to assume isothermal and isobaric nucleation. This is discussed in more detail in II.A, where the experimental time Δt_N is introduced. Applying the condition of criticality to Eq. 3 yields

$$\begin{aligned} \left(\frac{\partial \Delta G}{\partial V}\right)_{T,P,N} &= (P_l - P_v) + \sigma\left[\frac{dA}{dV}\right] + \left[\frac{d\sigma}{dV}\right]A = \\ (P_l - P_v) &+ \sigma\left(\frac{dA}{dr}\right)\left(\frac{1}{\frac{dV}{dr}}\right) + \left(\frac{d\sigma}{dr}\right)\left(\frac{1}{\frac{dV}{dr}}\right)A \end{aligned} \tag{4}$$

If the embryos of the new phase are assumed to be spherical, Eq. 4 becomes the generalised Laplace equation

$$P_v - P_l = \frac{2\sigma}{r} + \left(\frac{d\sigma}{dr}\right) \tag{5}$$

where r is the radius of the bubble embryo. A similar differential analysis of Eq. 3 for $\left(\frac{\partial \Delta G}{\partial N_v}\right)_{T,P,N_s}$ and $\left(\frac{\partial \Delta G}{\partial N_s}\right)_{T,P,N_v}$ will yield conditions of chemical equilibrium $\mu_l = \mu_v = \mu_s$.

Equation 5 states that the free energy of bubble formation is size dependent via the surface energy term. The value of $\left(\frac{d\sigma}{dr}\right)$ in Eq. 5 depends on the placement of the dividing surface (DS), i.e. the theoretical boundary between liquid and vapour phases that is set when modelling the system. The choice of dividing surface is one that establishes a connection between the mathematical model and experimentally measurable quantities, as well as providing meaningful simplification of the problem (29).

In this work, we choose the surface of tension (SoT) as the dividing surface. This choice assumes that liquid and vapour phases are separated by a spherical membrane with no rigidity and uniform tension across the surface. It is the only case where the surface tension is the same as the specific surface energy of a spherical embryo (29). By making this choice, we are assuming that the thermodynamic and mechanical definitions of the SoT are the same. The most important feature of the SoT is that it is defined such that $\left(\frac{d\sigma}{dr}\right) = 0$ and Eq. 5 is simplified to the Laplace equation of mechanical equilibrium $P_v - P_l = \frac{2\sigma}{r}$ (28).

The size-dependent energy barrier for the creation of a stable phase in a metastable fluid is then given by the work of nucleation. Replacing conditions of unstable equilibrium into 4 yields

$$W^* = \Delta G^* = \left(\frac{1}{3}\right)\sigma 4\pi r^{*2} \tag{6}$$

where r^* is the radius of the critical nucleus and an asterisk denotes critical values. In terms of the pressure in the liquid and vapour phases:

$$W^* = \left(\frac{16\pi}{3}\right)\frac{\sigma^3}{(P' - P_l)^2} \tag{7}$$

Where P' is the internal pressure in a critical nucleus. This form of the critical work of nucleation has been extensively used in recent works on bubble nucleation in liquids (21,26,30).

The critical work for nucleation is then used to predict the nucleation rate. This is the net rate at which bubbles reach a critical size. The critical size defines a maximum in W^* where nuclei have equal chances of growing or collapsing. The nucleation rate is proportional to the difference between the forward rates of vaporisation and the backward rates of condensation when the effects of viscosity and inertia are neglected (28,31).

Assuming that the timescales of nucleation are much shorter than the tensile period of the ultrasound wave, the nucleation rate can be approximated as a stationary quantity (21). At the critical size, the steady-state nucleation rate is usually represented as (21,26,28,32,33)

$$J_{ss} = J_0 \exp\left(-\frac{W^*}{k_B T}\right) \tag{8}$$

In this equation, the pre-exponential term J_0 accounts for the average kinetic and spatial properties of nucleation in that particular liquid. It also mathematically defines the upper bound for the nucleation rate since $\lim_{W^* \to 0} J_{ss} = J_0$. By neglecting the effects of viscosity and inertia in the liquid (31), J_0 can be defined in the form $J_0 = N_0\sqrt{\frac{2\sigma}{\pi m}}$, having $N_0 = \rho_L/m$ where ρ_L is the liquid density and m is the molecular mass of the liquid.

J_0 has units of nuclei per unit volume and per unit time.

A. Nucleation Pressure Thresholds for Histotripsy

When the peak negative ultrasound pressure generates sufficiently high nucleation rates, the focal volume cannot be considered a single-phase control volume anymore. The pressure and temperature pair at the ultrasound focus are then defined as the nucleation threshold of this liquid. For steady-state nucleation, the number of critical nuclei Σ formed in a focal volume V_0 during a time interval Δt_N can be approximated by

$$\Sigma = V_0 \int_0^{\Delta t_N} J_{ss}(P_l, T)dt \approx J_{ss}^* V_0 \Delta t_N \tag{9}$$

where J_{ss} is the nucleation rate in a liquid at a pressure P_l and temperature T (34). The quantity Δt_N can be referred to as the "experiment/observation time" at the steady state (26). This is a quantity that refers to the length of time where the medium is in a metastable state and does not relate to material properties. Given that intrinsic histotripsy is a threshold phenomenon, this quantity defines a fraction of the tensile wave where the medium is exposed to thermodynamic conditions that induce bubble nucleation. Eq. 9 then relates intrinsic material properties in the calculation of J_{ss} to experimentally verifiable quantities such as $\Delta t_N, V_0$ and Σ.

The choice of Δt_N is one that guarantees that the control volume's pressure and temperature are kept fairly constant at the threshold of nucleation within the rarefactional part of the wave. As an approximation of this time window, Δt_N is set as a tenth of the wave period as $\Delta t_N = \left(\frac{1}{10f}\right)$. The choice of Δt_N has the nucleation time-lag, which is of the order of nanoseconds for vapour bubble nucleation, as a lower bound. The upper bound of Δt_N is the period of the tensile part of the ultrasound wave.

Considering the formation of the first Σ nuclei, we can define

$$J_{ss}^* = \frac{\Sigma}{V_0 \Delta t_N} \tag{10}$$

where J_{ss}^* is the detectable nucleation rate for the appearance of Σ nuclei in a volume V_0 after Δt_N seconds. In this equation, V_0 is a control volume where Σ bubbles nucleate after Δt_N seconds, and its value is approximated as the volume within the 3 dB drop in intensity around the transducer focus (21).

Having the nucleation rate J_{ss} that forms the first Σ nuclei in a time-volume setup $V_0 \Delta t_N$, a phenomenological approximation to the nucleation pressure threshold of a liquid can be obtained by solving Eqs. 8 and 10 in terms of the pressure in the liquid P_l. This approach for obtaining the temperature-dependent nucleation pressure threshold $P_l^N(T)$ was first employed in (34) and has also been used in more recent work in bubble nucleation (26,35). Equating Eqs. 8 and 10, replacing the critical work of nucleation given by Eq. 7 and solving for P_l gives

$$P_l^N = P_v - \frac{1}{\zeta}\left(\frac{16\pi\sigma^3}{3k_BT\ln\left(\frac{J_0V_0\tau_s}{\Sigma}\right)}\right)^{\frac{1}{2}} \qquad (11)$$

P_l^N is the nucleation pressure P_l in the liquid at which an average of Σ nuclei appear during a time interval Δt_N in a focal volume V_0 at a temperature T. The Poynting correction ζ allows the temperature dependent VLE pressure of the liquid P_v to be used instead of the nucleus internal pressure P'. This is such that $\zeta = 1 - \left(\frac{\rho_v}{\rho_l}\right) + \frac{1}{2}\left(\frac{\rho_v}{\rho_l}\right)^2$, where ρ_v and ρ_l denote the saturated densities of vapour and liquid water, respectively. In the calculation of ζ, the IAPWS (36) equations for the densities of the saturated liquid ρ_l and vapour phases of water ρ_v were employed as

$$\frac{\rho_l}{\rho_c} = 1 + b_1x^{\frac{1}{3}} + b_2x^{\frac{2}{3}} + b_3x^{\frac{5}{3}} + b_4x^{\frac{16}{3}} + b_5x^{\frac{43}{3}} \\ + b_6x^{\frac{110}{3}} \qquad (12)$$

and

$$\ln\left(\frac{\rho_v}{\rho_c}\right) = c_1x^{\frac{2}{6}} + c_2x^{\frac{4}{6}} + c_3x^{\frac{8}{6}} + c_4x^{\frac{18}{6}} + c_5x^{\frac{37}{6}} \\ + c_6x^{\frac{71}{6}} \qquad (13)$$

In Eqs. 12 and 13, $x = 1 - \frac{T}{T_c}$, where T_c is the critical temperature and ρ_c the critical density of water. The values for constants b given by $b_1 = 1.99274064$, $b_2 = 1.09965342$, $b_3 = $ -0.510839303, $b_4 = $ - 1.75493479, $b_5 = $ -45.5170352, $b_6 = $ -6.74694450×10⁵.

The values of c are as follows $c_1 = $ -2.03150240, $c_2 = $ -2.68302940, $c_3 = $ -5.38626492, $c_4 = $ -17.2991605, $c_5 = $ -44.7586581, and $c_6 = $ - 63.9201063.

B. The Surface Tension of Histotripsy Nuclei

Inspection of Eqs. 7 and 11 will show that the liquid's surface tension is a key parameter in obtaining appropriate numerical predictions with the classical theory. CNT calculations within a capillary approximation predict that water can be stretched to underpressures of -140 MPa before nucleation takes place (37). This directly contrasts to literature data on bubble nucleation in acoustic fields, where experiments often do not surpass pressures of -40 MPa (15,16,21,22,26) for frequencies in the low MHz range.

This mismatch is caused by the default assumption that a capillary approximation is intrinsic to CNT, rather than a heuristic modelling choice (38). A capillary approximation is an implementation of the classical theory which uses the bulk surface tension of a planar liquid-vapour interface as an approximation to the surface tension of nanoscopic nuclei. As established by Gibbs phase rule, the bulk surface tension of pure water depends only on the system's temperature (39).

According to the IAPWS (39), the flat interface surface tension of pure water is given by

$$\sigma_\infty(T) = d_1x^{d_2}(1 + d_3x), \qquad (14)$$

where $x = 1 - \frac{T}{T_c}$, $d_1 = 235.8 \times 10^{-3}$ Nm⁻¹, $d_2 = $1.256 and $d_3 = $ -0.625.

As an alternative to the capillary approximation, it has been shown that a simple scalar correction of the bulk surface tension or the critical work of nucleation can harmonise CNT predictions and experimental pressure thresholds. Nucleation rates obtained in HIFU experiments at 1.1 MHz in purified water have been used in Eq. 11 in order to approximate an "effective value" of σ_∞ up to temperatures of 200 ˚C (21). These experiments showed that using a surface tension approximated by 23.7% of σ_∞ could predict HIFU nucleation pressure thresholds in CNT with a good agreement to experimental results. Similar experiments with a focus in histotripsy applications have been performed up to 90˚C (15), reporting scalar corrections between 25 and 27.5% of σ_∞.

More recently, pressures of about -100 MPa were reached inside water droplets by reflecting shockwaves generated by X-ray pulses (40). The transient tensions used in these experiments were of about 30 to 40 fs, which are five to six orders of magnitude shorter in duration than those produced by ultrasound in the Mega Hertz range. The difference in negative pressures achieved in both sets of experiments is probably caused by the significant difference in experiment duration and volume targeted.

For experiments in the low MHz range, the value of J_{SS}^* is of about $1.16\cdot10^{16}$. Contrastingly, the above-mentioned water droplets experiments yield detectable nucleation rates about ten orders of magnitude higher, with values of J_{SS}^* around $4.78\cdot10^{26}$. This study concluded that the short timescales of decompression could have been responsible for outrunning potential heterogeneous nucleation events in water, being then able to reach negative pressures of higher amplitude (40).

Based on this, we approach the modelling of the surface tension of water for bubble nucleation from a theoretical perspective with physical and empirical reasoning. If any substrates (impurities) of whatever origin are present in the fluid, the free energy of embryo formation takes a different form to that shown in Eq. 3:

$$\Delta G = G - G_0 + \Delta\phi_s. \qquad (15)$$

In this equation, the term $\Delta\phi_s = \phi_s - \phi_s^0$ accounts for the variation of the substrate's surface energy before and after nucleation. Substrates are different phases or molecular species which might act as preferential nucleation sites in the metastable phase.

For the case of pure substances, when no substrates are present, $\Delta\phi_s = 0$ and homogeneous nucleation is said to happen. If any foreign substances are present, HON will still be energetically favoured whenever $\Delta\phi_s > 0$, where the substrate is said to be of the stabilising type (21). This might also be the

case for experiments where the experimental volume V_0 is targeted for timescales Δt_N that are too short to enable the effect of impurities in water (40). Alternatively, if $\Delta\phi_s < 0$, heterogeneous nucleation will be the energetically favoured process. This is the case of impurities within liquids, such as spherical impurities, solid crevices and contact of different surfaces, which will be preferential nucleation sites because nucleation is less energetically demanding on at the given timescales over the volume of the experiment.

Following from this reasoning, a temperature-dependent activity factor for the surface tension might harmonise CNT predictions and experimental results, accounting for the effects of pressure, nucleus radius and temperature on the surface tension, as well as any potential ubiquitous impurities (22). This takes into account both the temperature-dependence of the process, as well as the possible dependence of the surface tension on the bubble embryo's size accounted for in Eq. 5.

The effective surface tension then takes the form $\sigma_E = \Psi\sigma_\infty$, where Ψ is an activity factor depending on the geometry, size, surface energies and wetting angle of the substances in question. This is a universal formulation, that when parametrised via experiments might be able to account for both HON and HEN simultaneously for a specific fluid (31,41). Herein, we build onto previous work (14) where a temperature-dependent activity factor Ψ_E is calculated by optimising the absolute error $E(P_l^N, T)$ between analytic predictions of Eq. 11 and experimental data for nucleation pressure thresholds in acoustic fields from aforementioned studies (15,21,42):

$$E(P_l^N, T) = \left| P_l^N\big(T, \Psi_E(T)\big) - P_{EXP}(T_{EXP}) \right| \qquad (16)$$

where P_{EXP} and T_{EXP} represent, respectively, experimental values of the nucleation pressure threshold and the temperature at which they were obtained.

The data used for parametrisation was mainly based on three studies and two different techniques. The data from (15,21) were obtained via ultrasound-induced bubble nucleation. In these sets of experiments, 2 to 6 cycles generated from a 1.1 MHz piezoelectric transducer were applied to a water sample of approximate volume $2.1 \cdot 10^{-4}$ mm^3. Both sets of experiments were performed in purified, degassed water. Discussion in (21) highlighted the low sensitivity of the experiment to gas content, which was obtained for results averaged over 100 pulses, whilst in (15), results were recorded over a single pulse. The data obtained from (42) was obtained by centrifugation. This method consists of rotating a tube filled with water at very high speeds such that negative pressures are developed on the rotating axis due to centrifugal forces. For the centrifuge method, the results used were those obtained at temperatures between 20 and 50 ˚C in a water sample of volume 0.38 mm^3 (26).

C. Numerical Simulation of Histotripsy Pressure and Temperature Fields

The HITU Simulator (43) was used to solve a wide-angle parabolic approximation of the generalised one-way Westervelt equation and obtain 2D axisymmetric pressure waveforms along the propagation axis and the radial direction. The HITU Simulator also models HIFU-induced temperature rises through Pennes' Bioheat Transfer Equation (BHTE). Both the Westervelt equation and the HIFU Simulator have been extensively used in previous efforts to model boiling histotripsy pressure and temperature fields (13,14,44,45).

The acoustic simulations were performed individually for two single-element bowl-shaped transducers operating at 2 and 1.1 MHz (Sonic Concepts H148 and H102) for input electrical powers ranging from 100 to 300W assuming 85% transducer efficiency. Acoustic propagation was numerically evaluated for 5.32 cm in water followed by 2.6 cm in liver tissue. The spatial grid for both acoustic and thermal simulations consisted of 10 elements per wavelength in the axial direction and 15 elements per wavelength in the radial direction. Material parameters and physical properties were obtained from previous works in the literature (46), and the initial condition for the BHTE simulations was such that $T_0 = 20$ °C.

TABLE I

PARAMETERS FOR THE HITU SIMULATOR.

Property	Water (47)	Liver (46,48)
Speed of sound (m·s^{-1})	1482	1575
Mass density (kg·m^{-3})	1000	1060
Attenuation at 1 MHz (dB·m^{-1})	0.217	52
Power of attenuation vs. frequency curve	2	1.1
Nonlinearity coefficient	3.5	4.5 - 6.8

TABLE II

PARAMETERS FOR THE BHTE SIMULATIONS.

Property	Water (47)	Liver (47,48)
Specific heat (J·kg^{-1}·°C^{-1})	4180	3628
Thermal conductivity (W·m^{-1}·°C^{-1})	0.6	0.57
Blood perfusion rate (kg·m^{-3}·s^{-1})	-	0 – 19

III. RESULTS AND DISCUSSION

D. Pressure Thresholds and Nucleation Rates in Histotripsy

In order to calculate an activity factor for the surface tension of water, P_l was calculated via Eq. 11, V_0 was approximated as

an ellipsoidal focal volume within the - 3dB intensity drop region for a 2 MHz HIFU transducer (Sonic Concepts H148) such that $V_0 = 1.73$ m^3. Δt_N is set as a tenth of the ultrasound wave period $\Delta t_N = \left(\frac{1}{10f}\right) = 5 \cdot 10^{-8}$ s. Fig. 1 shows the error $E(P_l^N, T)$ associated with obtaining values for Ψ_E, which ranged between 0.26 and 0.32. A regression curve was fit to this data, such that for temperatures between 0 and 90 °C Ψ_E is given by:

$$\Psi_E(T) = 0.4869 - 6.1425 \cdot 10^{-4}(T + 273.15) \quad (17)$$

Throughout this work, for calculations at temperatures between 90 and 110 °C, Ψ_E was extrapolated based on Eq. 17 with $R^2 = 0.7374$. For temperature values above 110 °C a conservative approach is taken and a constant $\Psi_E(T > 110°C) = \Psi_E(110°C)$ is assumed.

Nucleation pressure thresholds are plotted as a function of temperature in Fig. 2, comparing the effects of the scaling quantity Ψ_E on the values of the nucleation pressure threshold. Asterisks represent experimental data for HIFU-induced bubble nucleation taken from the literature (15,21). By employing the linear approximation for Ψ_E shown in Eq. 17, it is possible to obtain pressure thresholds which are in close agreement with values reported in the literature throughout a temperature range of interest in HIFU applications. Previously reported values for Ψ_E are shown to underestimate the magnitude of P_l^N at low temperatures and to overestimate it at higher temperatures. This figure also provides a prediction of temperature-dependent nucleation pressures for intrinsic histotripsy approaches at physiological temperatures.
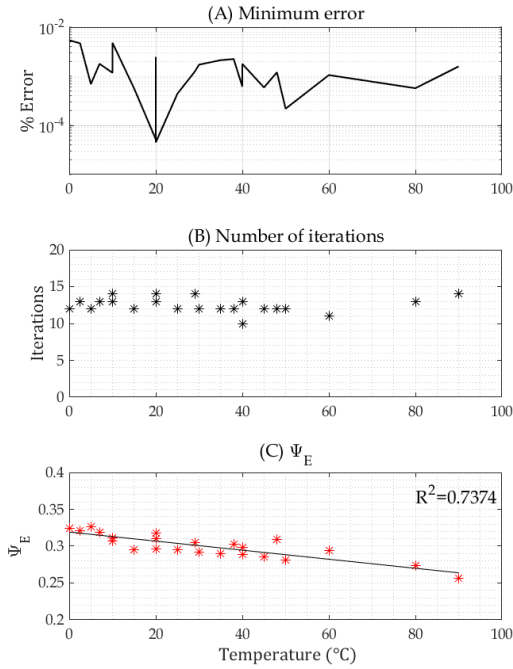

Figure 1. Error minimisation parameters for obtaining Ψ_E. (A) Percent error between analytical predictions and experimental values of P_l^N. (B) Number of iterations needed until minimum error was found. (C) Values of Ψ_E and linear regression of points.
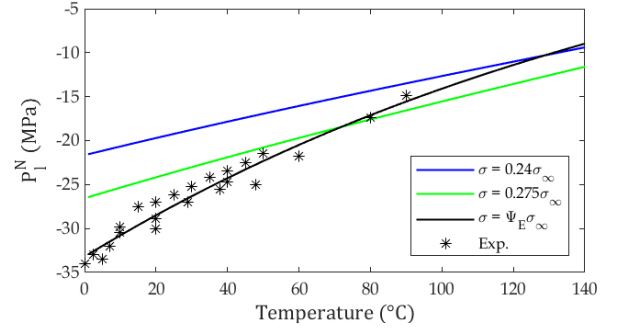

Figure 2. Comparison between CNT predictions of P_l^N at different Ψ_E. Blue and green curves represent a constant Ψ_E, 0.24 and 0.275 respectively, and black curve represents a temperature-dependent Ψ_E shown by Eq. 3.42. Asterisks denote experimental values of Ψ_E obtained from the literature (15,21,22).

In Fig. 3, the steady-state nucleation rate given by Eq. 8 is plotted as a function of temperature for three pressure contours (-30, -15 and -5 MPa) in 3-A, and as a function of pressure for three temperature contours (40, 100 and 200 °C) in 3-B. These values are in units of the number of bubble nuclei per meter cubic per second. Bubble nucleation takes place whenever the contours in these plots reach the value for J_{ss}^* in Equation 10, which is of about $1.16 \cdot 10^{16}$ for the 2 MHz transducer used in the modelling of nucleation in section III.B. This means that the values shown in these figures are realistic for $J_{SS} \leq 1.16 \cdot 10^{16}$ but of theoretical interest otherwise, since the control volume in question is not a single-phase fluid anymore. The following analysis and discussion are then useful for exploring mathematical and physical trends in bubble nucleation.

Fig. 3-A shows that at -15 MPa, nucleation rates grow by 20 orders of magnitude in the temperature interval 60°C and 100°C. However, at temperatures lower than 50°C, nucleation rates are only appreciable at very large negative pressures such as -30 MPa. At high temperatures (100 – 200 °C) in 3-B, nucleation rates plateau and present little change as the pressure in the liquid is decreased. In this case, J_{ss} assumes asymptotic behaviour, close to its saturation value J_0. These trends show that at low temperatures the ultrasound pressure is the fundamental trigger for bubble nucleation (cavitation), but at high temperatures, heating of the medium will increasingly control nucleation.
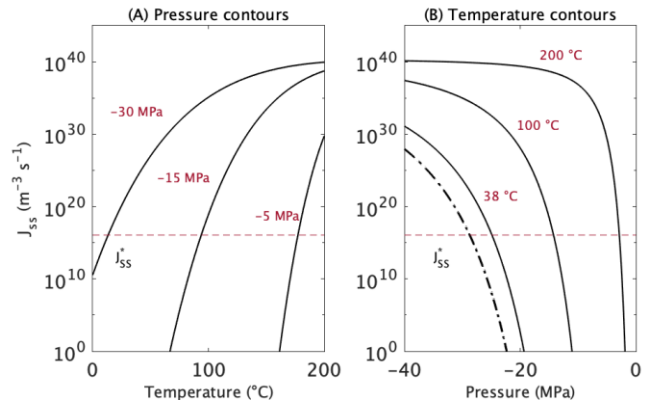
Figure 3. (A) Nucleation rate as a function of temperature with pressure contours. (B) Nucleation rate as a function of pressure with temperature contours. The dot-dashed curve in (B) represents room temperature.

The terms boiling and cavitation are traditionally used to describe bubble formation in liquids, many times without explicit distinction between them. It has been proposed that the nomenclature "boiling" should only be used for cases where nucleation is triggered by a superheat $\Delta T > 0$ at constant liquid pressure. Conversely, cavitation would be the phenomenon caused by a "tension", also termed underpressure (31), $\Delta P_l = P_v - P_l \geq 0$ at constant temperature.

In practice, it is difficult to design experiments which isolate the effects of both thermodynamic variables and the distinction between the two phenomena is not clear (49). At temperatures sufficiently close to a liquid's thermodynamic limit of superheat $(T \approx 0.89\,T_c)$ nucleation rates increase approximately three or four orders of magnitude per degree Celsius. In such cases it is appropriate to talk about boiling and a heating dominated process (50). Contrastingly, away from the thermodynamic limit of superheat $(T < 2T_c/3)$, nucleation rates are only appreciable at large negative pressures (51). This happens because $P_l \gg P_v$, therefore the temperature-dependence of nucleation on the exponent of Equation 8 is greatly reduced. At these conditions, it is meaningful to discuss the temperature-dependent tensile strength of a liquid and term the process as cavitation.

Although these physical trends elucidate differences between the extrema of boiling and cavitation regimes, it becomes clear that this distinction might seem insufficient to account for the physics of shock-scattering histotripsy. This is a form of histotripsy that depends on the nucleation or pre-existence of a gas pocket around the ultrasound focus, which reflects the incoming non-linear field, causing a pre-focal cavitation cloud (52). We do not attempt to further frame this form of nucleation event in the present model due to uncertainties related to a range of factors in shock-scattering histotripsy experiments, these include: (i) the nature of such pre-existing/naturally occurring gas bubbles and their replicability in *in vivo* experiments and (ii) the acoustic field that results from the reflection of shockwaves on a gas bubble surface.

It should be noted, however, that boiling histotripsy experiments in tissue phantoms captured by high-speed camera imaging have indicated that the formation of the "head" of a boiling histotripsy lesion could be caused by cavitation generated by backscattered pressures below the tissues' intrinsic pressure threshold (45). Further modelling on the magnitude of the backscattered acoustic field from boiling histotripsy bubbles has shown that negative pressures of -31.6 MPa might be achieved due the existence of a 1.5 mm radius bubble at the ultrasound focus. This suggests that, in boiling histotripsy, the formation of a pre-focal cavitation cloud depends on the size and location of the initial boiling bubble as well as the constructive interactions of the incident and backscattered fields. These events of nonlinear wave propagation and scattering were modelled using the k-Wave MATLAB toolbox. The authors also clearly mention a possible limitation of this study which is a lack of work validating k-Wave in capturing highly distorted nonlinear waves in heterogeneous media (53).

The quantity Δt_N defines the time interval over which the first Σ bubbles nucleate. This quantity should be a fraction of the wave period and is estimated from the ultrasound frequency used (54). The choice of Δt_N needs to be such that variations in P_l and T are minimal and these quantities can be assumed nearly constant. The parameter V_0 represents the experimental volume, i.e., the volume of the nucleating system under consideration. For nucleation induced by focused transducers, this parameter can be approximated by the focal volume of the transducer being used, e.g. based on the -3 dB criterion previously described.
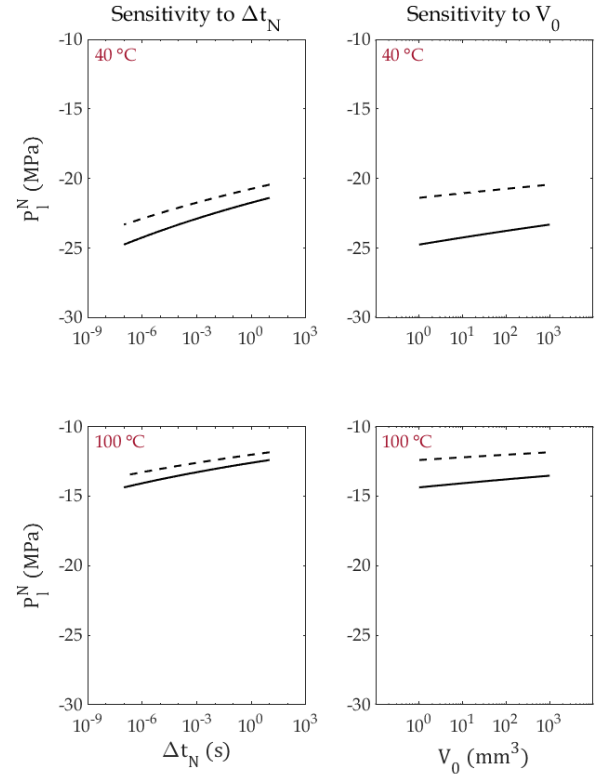

Figure 4. The effects of Δt_N (left column) and V_0 (right column) on P_l^N. Results in top row are obtained for $T = 40\ ^\circ C$, results in bottom row are obtained for $T = 100\ ^\circ C$. Dashed and solid lines represent the range of variation of P_l^N for V_0 (1 - 1000) mm^3 in the first column and for Δt_N ($10^{-6} - 1$) s in the second column.
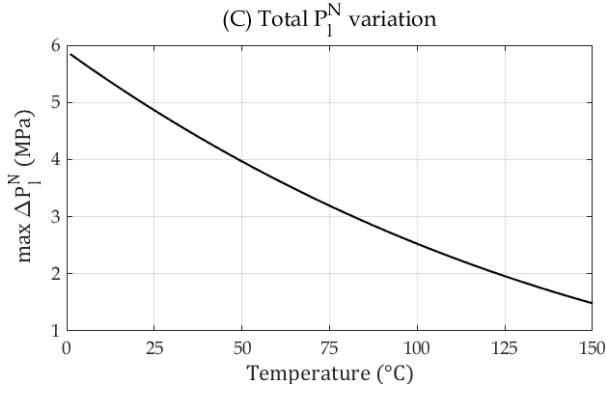
Figure 5. Maximum variation in $P_l^N(T)$ caused by the parametrisation of Δt_N and V_0.

By varying Δt_N between 1 μs and 1 s in Eq. 11 it was found that the magnitude of the nucleation pressure threshold monotonically decreases with increasing Δt_N. Similarly, by varying V_0 between 1 mm^3 and 1 cm^3 P_l^N also decreases monotonically with increasing V_0. This trend indicates that, at constant temperature, bubble nucleation is favoured at lower frequencies, since these would imply longer Δt_N and larger V_0. In Fig. 5, the maximum difference $\Delta P_l^N = |P_l^N(1\,s, 1\,cm^3) - P_l^N(1\,\mu s, 1\,mm^3)|$ observed by varying V_0 and Δt_N in the evaluation of P_l^N as predicted by Eq. 11 is plotted. This figure shows that the effects of Δt_N and V_0 are shown to decrease at high temperatures. This leads to the conclusion that parameters like the ultrasound frequency and the focal volume of the transducer have a more important effect when nucleating bubbles at low temperatures: Transducers with lower frequencies and larger focal volumes would then favour bubble nucleation.

E. Spatial-Temporal Trends of Nucleation in Boiling Histotripsy

Baseline acoustic simulations used 10 points per wavelength in the axial direction and 15 points per wavelength in the radial direction in the discretisation of the grid. There is no rule defining the exact number of harmonics needed for obtaining accurate solutions of the Westervelt equation (43). Convergence tests were carried to define the ideal number of harmonics to be used in the simulations. Acoustic fields were computed at 32, 64, 128, 256, 512, 1024 and 2048 harmonics at 150 W input electrical power and assuming 85% efficiency for the 2 MHz transducer and at 300 W for the 1.1 MHz transducer. Convergence was assumed whenever doubling the number of harmonics resulted in a step increase smaller than 5% for key acoustic quantities such as heat deposition rate, acoustic intensity and peak negative focal pressure.

Key acoustic quantities in the calculation of nucleation pressure thresholds such as the focal peak negative pressure and focal heating rates converged monotonically for increasing number of harmonics used in the simulations. At 512 harmonics, results were found to be within 5% error from simulations at 256 harmonics, thus simulations throughout this manuscript were performed at 512 harmonics for both transducers. Quantities such as the acoustic intensity and focal peak negative pressure were less sensitive to the number of

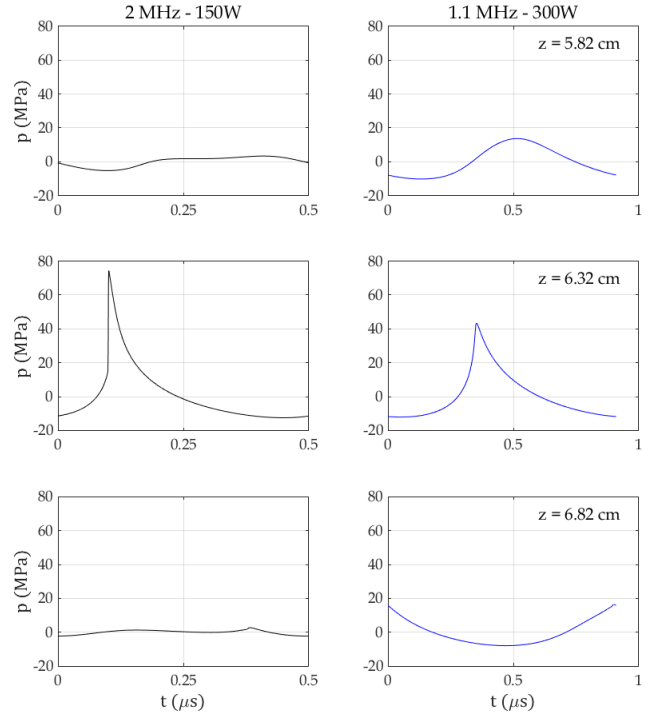harmonics used in the simulations than focal heating rates.

Figure 6. Pressure waveforms around the ultrasound focus.

Results in section III showed that HIFU-induced nucleation pressure thresholds can be modelled as a function of temperature upon appropriate parametrization of the medium's surface tension. Eq. 11 was used to predict the nucleation pressure threshold at the point of highest temperature (obtained with the Bioheat equation) within the HIFU focus as a function of sonication time. Fig. 7 shows focal nucleation pressure thresholds for input electrical powers of 100, 150 and 200 W for a 2 MHz transducer and 200, 300 and 400 W for a 1.1 MHz transducer. Having that the focal peak-negative pressure also depends on the electrical power provided to the transducer, these were indicated by red asterisks in the respective electrical power contour.
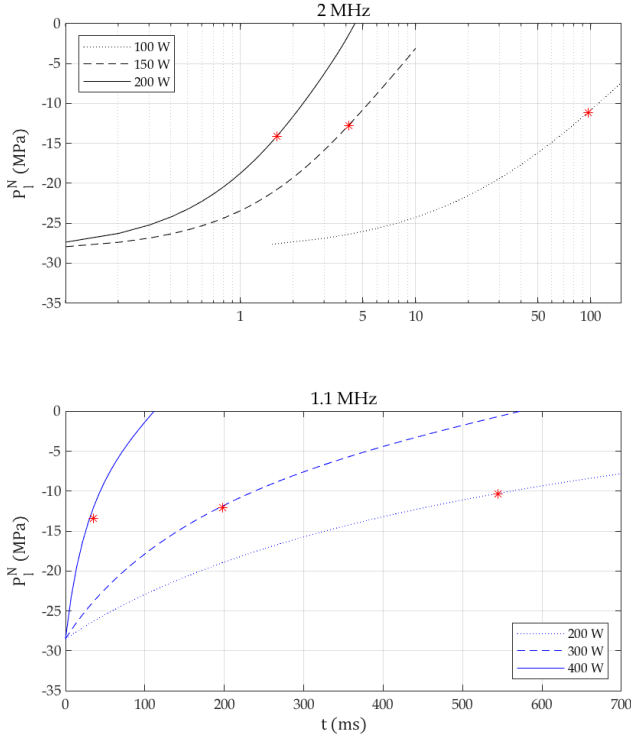
Figure 7. Focal nucleation pressure thresholds as a function of pulse length (sonication time). Red asterisks denote focal peak-negative pressures for the equivalent input electrical power.

Following from the underlying assumptions in the derivation of Eq. 11, nucleation will happen in a time interval $\Delta t_N = (1/10f_0)$ after the focal nucleation pressure threshold is equal to the focal peak-negative pressure. These results show that the time needed for the nucleation of a boiling bubble decreases as heating rates are increased and as focal peak-negative pressures are lowered. Propagation at 1.1 MHz results in much longer times needed for bubble nucleation since heat deposition at these conditions is one to two orders of magnitude lower that at 2 MHz for lower input electrical powers.

Traditionally, the pulse-length required for nucleation has been modelled as the time that the HIFU focus takes to reach 100 °C in the presence of shocks. By evoking weak shock theory (12,55), it is possible to approximate focal heating rates in focused ultrasound beams as

$$Q_{WS} = \frac{\beta f_0 (\Delta p)^3}{6\rho_0^2 c_0^4} \tag{18}$$

where Δp is the magnitude of the incoming shock. The "time-to-boil" t_b can then be estimated by neglecting both diffusion and perfusion in the Bioheat Transfer equation, which reduces to (12,56):

$$Q_{WS} t_b = \Delta T \rho C \tag{19}$$

This analytical model uses heating rates obtained from weak shock theory to approximate the time needed for boiling to occur, by assuming that boiling is pressure-independent and

always occurs at 100 ˚C independently of the liquid pressure and gas concentration.

An estimation of the timescales required of boiling histotripsy that accounts for the effects of the ultrasound focal peak-negative pressure can be achieved with the aid of CNT. Since the nucleation pressure is a temperature-dependent quantity, the nucleation pressure threshold can be calculated as function of HIFU-induced heating as displayed in Fig. 7. This involves solving in time an equation of the type $p^- = P_l^N \left(T_{peak}(t) \right)$, where p^- is the focal peak-negative acoustic pressure, P_l^N is defined by Eq. 11 and T_{peak} is obtained with the solution of the Bioheat equation. This equation is solved numerically in time, recording the value of t at which $P_l^N = p^-$.

A comparison between the two approaches discussed above, as a function of input electrical power to the transducer, is shown in Fig. 8.
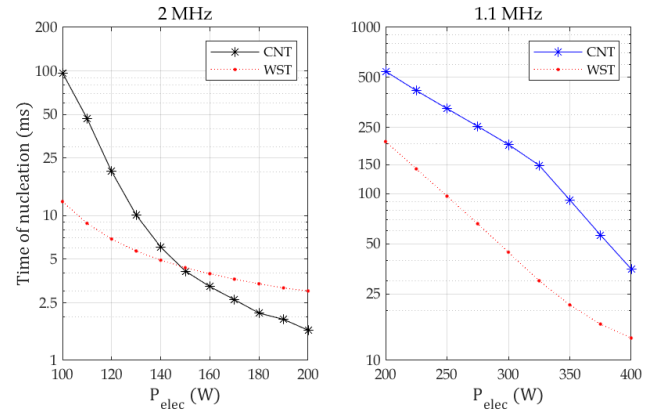

Figure 8. Time of nucleation as a function of input electrical power.

Figure 8 shows a comparison of the time of nucleation calculated via CNT and the time to reach 100 °C given by Eq. 19. The results shown in Fig. 8 for the weak-shock theory (WST) approach used the same formulation as previous experimentally-validated work (12), but were calculated by using physical constants displayed in Tables I and II which were also used to parametrise the CNT model.

Before discussing any contrast between the two approaches, it is necessary to highlight that these results are sensitive to the temperature-dependence of parameters such as ρ, c_0 and C, which in here were (i) assumed to be temperature independent, using values obtained at room temperatures, and (ii) heating-rate independent, since these materials might present temperature-dependent changes at timescales that are incompatible with millisecond heat deposition.

It can be seen that the time needed for nucleation decreases monotonically with increasing input electrical power for both transducers. In comparison with CNT results, the WST approach predicts longer times until nucleation at powers below 150 W for the 2 MHz transducer, and shorter times at powers above 150 W. For propagation at 1.1 MHz, WST always predicts shorter times required for nucleation if compared to CNT. Physically, the approximation in Eq. 19 might overestimate focal temperature rises by neglecting both heat

diffusion and perfusion. However, it is known that at the timescales characteristic of histotripsy, both effects have traditionally been neglected (57).

We would like to discuss the comparison between the two approaches as a hypothesis-formulating exercise in considering the physics that is accounted for when parametrising histotripsy experiments. It is also worth noting that a critical aspect in the evaluation of these results relies on an understanding of the prior distribution of bubble nuclei (12) as well as the concentration of dissolved gas in the medium.

Existing modelling work in WST has found good agreement between WST and experiments at high-intensity exposures, particularly at values of $t_b \leq 10$ ms (12). In these conditions, the differences between CNT and WST approaches found in the present work were relatively small for propagation at 2 MHz.

Nonetheless, the discrepancy in results shown in Fig. 8 might be caused by the fundamental assumption in WST that boiling always takes place at 100˚C, and by the absence of terms considering the pressure in the liquid. This would potentially lead WST to underestimate the time of nucleation in cases where nucleation happens at $T > 100$ °C and overestimate it in cases where nucleation happens at $T < 100$˚C.

It is now crucial to discuss the empirical knowledge that water always boils at 100˚C, and the reasons why this is not necessarily replicable, or true, when modelling bubble nucleation events, especially under ultrasound sonication in physiological or near-physiological media. We present three thoughts for the consideration of the reader:

(i) Untreated water systems in the real world are rarely depleted of impurities such as stabilised microbubbles, dissolved gas, or solid crevices where gas phases are trapped. At sea-level, the vapour pressure of water at 100˚C is virtually equal to the atmospheric pressure. This means that there will be increased water vapour transport through any pre-existing water-air interfaces at 100 ˚C. These interfaces might be the flat surface between water an air but might also be the curved interfaces between water and stabilised microbubbles, or between water and gas trapped in crevices.

(ii) The process of boiling at 100˚C in untreated water at atmospheric conditions is further amplified by the fact that the solubility of gases in water sharply decreases with increasing temperature (58). This means that the "boiling" process that is empirically observed at 100˚C is not purely boiling, it is also a process of dissolved gas coming out of solution due to saturation of these gases that is caused by temperature rises. The pre-existence of a water-air interface added to the combination of vaporisation and gas dissolution then results in significantly higher rates of mass transfer between liquid and vapour phases.

(iii) In his landmark work on thermodynamics, Josiah Willard Gibbs has shown that the critical work needed for bubble nucleation in liquids is rooted in the energetic requirements of creating a surface in the bulk of a liquid (59). In the present formulation, this is demonstrated by Eq. 6, where the critical work of nucleation W^* is surface, rather than volume, dependent (31). This means that most of the energetic demand for nucleation is imposed by the creation of a liquid-vapour interface in a system assumed single-phased, rather than by mass transfer between two pre-existing phases. The latter process is better accounted for by bubble dynamics approaches, as discussed in the introduction of this work.

In light of points i-iii, the demand for a theoretical framework of bubble nucleation that simultaneously accounts for the effects of liquid pressure, temperature and gas composition becomes clear. Furthermore, the demand for a hybrid approach where CNT can account for hydrodynamic terms, such as those treated in Rayleigh-Plesset type equations, might also be needed for a universal understanding of fundamental mechanisms in HIFU-induced bubble nucleation.

Focal temperature profiles right after the moment of nucleation are shown in Fig. 9 for propagation at 2 MHz and 150 W input electrical power ($t \approx 4.8$ ms) and 1.1 MHz and 300 W electrical power ($t \approx 240$ ms). In both simulations, the highest temperatures were obtained slightly pre-focally and were in the range 100 – 120 °C. Heated regions were obtained as an ellipsoid around the HIFU focus. This spatial temperature profile is then used to calculate temperature-dependent nucleation pressure thresholds spatially, which can be seen in Fig. 10.
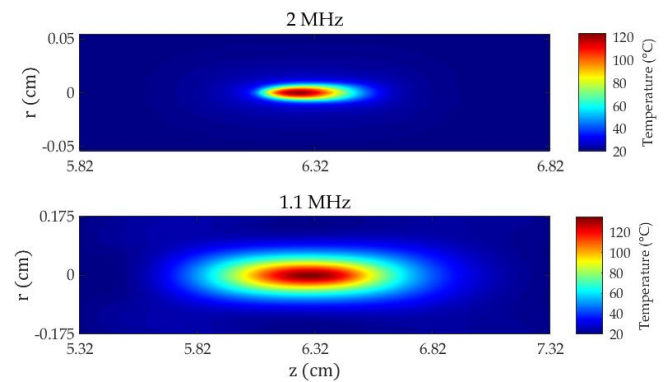

Figure 9. Focal temperature profile at the moment of nucleation. Top figure shows temperature distribution after 4.8 ms of sonication at 2 MHz and 150W input electrical power. The bottom figure shows temperature profiles after 240 ms of sonication at 1.1 MHz with 300W input electrical power.

The spatial distribution of the nucleation pressure threshold at the moment of nucleation shows contours of pressures with similar shape to those created by heat deposition. Nucleation then would take place within regions where the peak-negative acoustic pressure is below the pressure thresholds plotted. These results show that heat deposition not only facilitates nucleation by lowering pressure thresholds, but also creates preferential nucleation sites around the regions of highest temperature. High-speed camera imaging of optically transparent tissue mimicking gel phantoms has shown regions of highest heat deposition as the preferential site where vapour bubbles nucleate in boiling histotripsy (45).
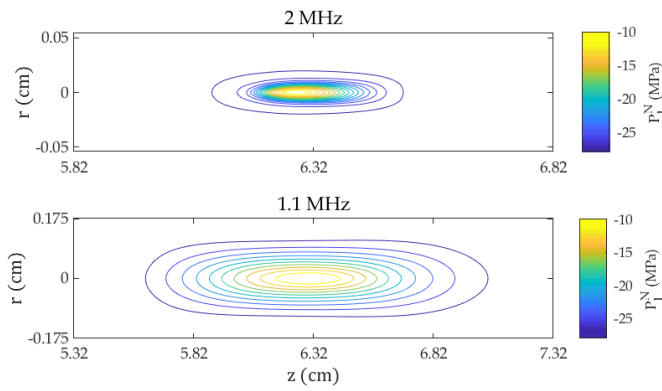
Figure 10. Temperature-dependent nucleation pressure thresholds at the time of nucleation. Top figure shows contours of nucleation pressure threshold distribution after 4.8 ms of sonication at 2 MHz and 150 W input electrical power. The bottom figure shows values of P_l^N after 240 ms of sonication at 1.1 MHz with 300 W input electrical power.

In both sets of results, a cigar-shaped region is observed, in agreement to previous numerical simulation of HIFU heat deposition and experiments in boiling histotripsy (45). It has been observed that boiling histotripsy lesions have a characteristic "tadpole" shape, consisting of a spherical "head" and an ellipsoidal "tail". This cigar-shaped nucleation region would be the location where the first boiling bubble(s) form, and start the process of mechanical fractionation of tissue (45).

Spatial profiles of the nucleation rate are plotted in Figs. 11 and 12, compared to spatial temperature profiles and peak-negative acoustic pressures in the focal region. These results show that the highest nucleation rates occur within a sub-volume of the HIFU focus, that coincides with the regions of highest temperature where the peak-negative pressure surpasses the nucleation pressure threshold. Interestingly, the bottom plot in Fig. 11 shows that although the lowest acoustic pressures happened slightly pre-focally, these were insufficient to generate appreciable nucleation rates due to lower temperature.
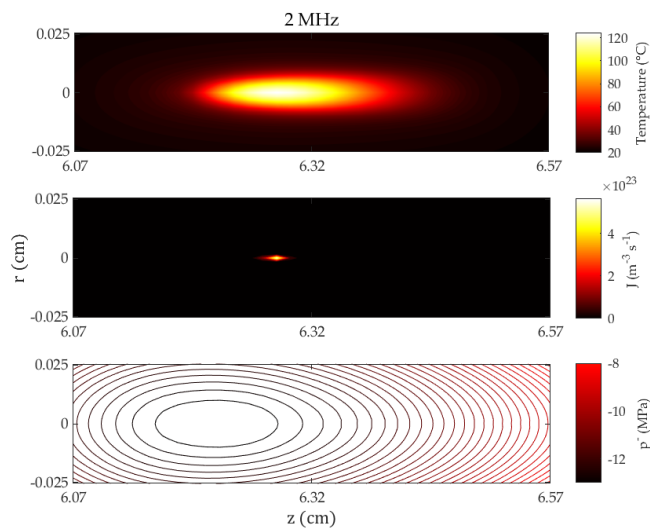

Figure 11. Overview of the bubble nucleation rate (middle figure) compared to temperature profiles (top) and peak negative acoustic pressures (bottom) at 4.8ms of sonication for propagation at 2 MHz and 150W input electrical power.
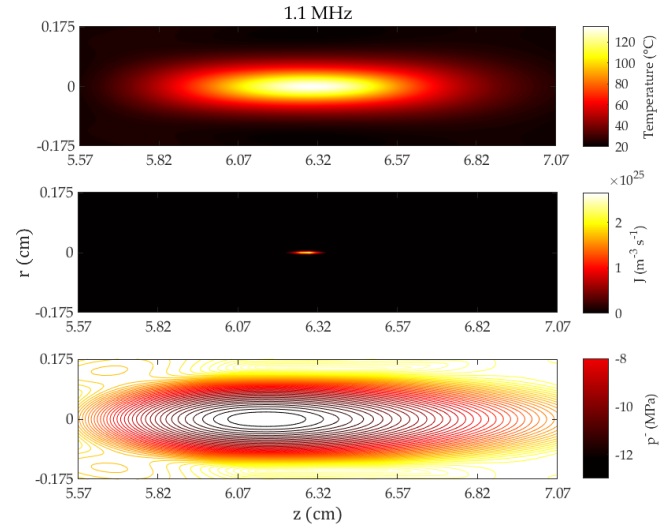

Figure 12. Overview of the bubble nucleation rate (middle figure) compared to temperature profiles (top) and peak negative acoustic pressures (bottom) at 4.8ms of sonication for propagation at 1.1 MHz and 300W input electrical power.

A similar trend was observed for both transducers simulated, having the preferential nucleation site within the regions of highest temperature. Since the nucleation pressure threshold is temperature-dependent, nucleation is spatially restricted to regions where the peak negative acoustic pressure overcomes the nucleation pressure threshold, however, these regions are not necessarily the regions of lowest acoustic pressure.

The size distribution of critical bubble nuclei at the HIFU focus, calculated with Laplace's equation for mechanical equilibrium is shown in Fig. 13. These range from 6 – 10 mm in both sets of results, where the size of critical nuclei increases towards the regions of highest heat deposition. These results agree with those found HIFU nucleation experiments in water (21). This implies that the HIFU focus is the location where bubble nuclei have higher chances of merging and forming larger bubbles which are mechanically stable within the thermodynamic conditions imposed by HIFU pressure and temperature fields.
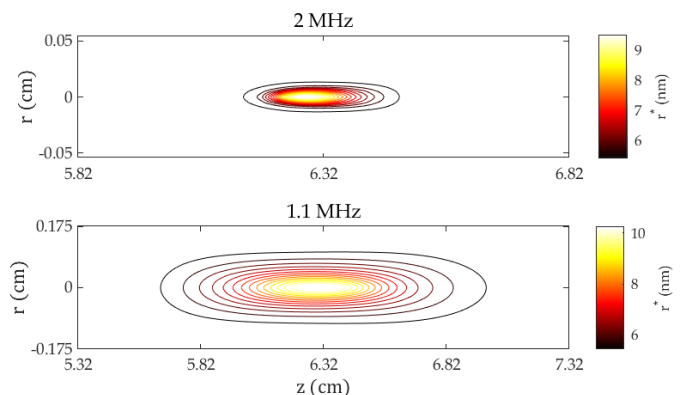

Figure 13. Size of critical nuclei at the moment of nucleation.

It is important to note that the ability of Laplace's mechanical

equilibrium equation to predict the size of critical nuclei shown in Fig. 13 has limitations. This is an equation that predicts the minimum size of bubble nuclei so that nucleation happens, under the assumption that the surface tension is size-independent. This equation does not take into account either inertial or viscous terms present in Rayleigh-Plesset-type equations for bubble dynamics (32). Numerical simulations on the growth of nanoscale boiling histotripsy nuclei have shown that they grow by vapour transport in the presence of fully developed incoming shocks (60). It has also been shown that the temperature field around these bubbles greatly limit their growth which is controlled by vapour transport (61,62).

After the growth of these bubbles to dimensions similar to the wavelength of the acoustic field, these bubbles act as reflectors creating regions of extremely low negative pressure pre-focally where a cavitation cloud occurs (45). Simulations of the interaction of shockwaves with a vapour bubble have shown that backscattered peak negative pressures range between -17.4 and – 31.6 MPa for focal vapour bubbles of 0.2 to 1.5 mm (53). These values are within and beyond the nucleation pressure thresholds predicted for the focal region and its vicinity in Fig. 10. It is thus possible that pre-focal cavitation cloud formation in boiling histotripsy is a threshold phenomenon that will ultimately depend on the dimensions of the boiling bubble and its interaction with the incoming field.

III. Conclusions

A thermodynamic model for bubble nucleation in HIFU was developed using classical nucleation theory. This model yields an estimate for the temperature dependence of the nucleation pressure threshold in water-like media, taking into account the ultrasound frequency and focal volume. Experimental data on HIFU nucleation was used in order to parametrise a temperature dependent activity factor for the surface tension of water which is capable of harmonising CNT predictions and pressure thresholds obtained in ultrasound experiments.

Results show that heat deposition in boiling histotripsy facilitates nucleation by decreasing focal nucleation pressure thresholds. With the present approach, it is possible to calculate the minimum pulse-length required to achieve vapour bubble nucleation, as well as estimating nucleation preferential sites and the size distribution of early bubble nuclei. The size of critical bubble nuclei was found to increase in regions of higher temperature within the HIFU focus, ranging from 6-10 nm. Furthermore, these results suggest that the pressure requirements of intrinsic-threshold histotripsy might be reduced by pre-heating the treatment zone up to 50 ˚C. Overall, results indicate that it is not possible to detach the effects of focal pressure and temperatures in the nucleation of bubbles.

References

1. Church CC. Spontaneous homogeneous nucleation, inertial cavitation and the safety of diagnostic ultrasound. Ultrasound Med Biol. 2002 Oct;28(10):1349–64.

2. Apfel RE, Holland CK. Gauging the likelihood of cavitation from short-pulse, low-duty cycle diagnostic ultrasound. Ultrasound Med Biol. 1991;17(2):179–85.

3. Crum LA, Hansen GM. Generalized equations for rectified diffusion. J Acoust Soc Am. 1982 Jan;72(5):1586–92.

4. Crum LA. Nucleation and stabilization of microbubbles in liquids. Appl Sci Res. 1982;38(1):101–15.

5. Stride E, Saffari N. Microbubble ultrasound contrast agents: A review. Proc Inst Mech Eng Part H J Eng Med. 2003;

6. Hynynen K, McDannold N, Vykhodtseva N, Jolesz FA. Noninvasive MR imaging-guided focal opening of the blood-brain barrier in rabbits. Radiology. 2001;

7. Holt RG, Roy RA. Measurements of bubble-enhanced heating from focused, MHz-frequency ultrasound in a tissue-mimicking material. Ultrasound Med Biol. 2001 Oct;27(10):1399–412.

8. Khokhlova VA, Fowlkes JB, Roberts WW, Schade GR, Xu Z, Khokhlova TD, et al. Histotripsy methods in mechanical disintegration of tissue: Towards clinical applications. Int J Hyperth [Internet]. 2015 Feb 17;31(2):145–62. Available from: http://www.tandfonline.com/doi/full/10.3109/02656736.2015.1007538

9. Ziemlewicz TJ, Jove JV, Serres X, Cannata J, Miller R, Duryea A, et al. THERESA Study: Final Reporting of Phase I Study of Safety and Efficacy of Hepatic Histotripsy. In: SIO2020 - Scientific Abstracts: Liver Metastases and Pancreas. 2020.

10. Bader KB, Vlaisavljevich E, Maxwell AD. For Whom the Bubble Grows: Physical Principles of Bubble Nucleation and Dynamics in Histotripsy Ultrasound Therapy. Ultrasound in Medicine and Biology. 2019.

11. Canney MS, Khokhlova TD, Khokhlova VA, Bailey MR, Ha Hwang J, Crum LA. Tissue erosion using shock wave heating and millisecond boiling in HIFU fields. In: AIP Conference Proceedings. 2010.

12. Canney MS, Khokhlova VA, Bessonova O V., Bailey MR, Crum LA. Shock-Induced Heating and Millisecond Boiling in Gels and Tissue Due to High Intensity Focused Ultrasound. Ultrasound Med Biol [Internet]. 2010 Feb;36(2):250–67. Available from: https://linkinghub.elsevier.com/retrieve/pii/S0301562909015385

13. Khokhlova TD, Canney MS, Khokhlova VA, Sapozhnikov OA, Crum LA, Bailey MR. Controlled tissue emulsification produced by high intensity focused ultrasound shock waves and millisecond boiling. J Acoust Soc Am. 2011;

14. de Andrade MO, Haqshenas SR, Pahk KJ, Saffari N. The effects of ultrasound pressure and temperature fields in millisecond bubble nucleation. Ultrason Sonochem. 2019;

15. Vlaisavljevich E, Xu Z, Maxwell AD, Mancia L, Zhang X, Lin KW, et al. Effects of temperature on the histotripsy intrinsic threshold for cavitation. IEEE Trans Ultrason Ferroelectr Freq Control. 2016;63(8):1064–77.

16. Maxwell AD, Cain CA, Hall TL, Fowlkes JB, Xu Z. Probability of Cavitation for Single Ultrasound Pulses Applied to Tissues and Tissue-Mimicking Materials. Ultrasound Med Biol. 2013 Mar;39(3):449–65.

17. Lin KW, Kim Y, Maxwell A, Wang TY, Hall T, Xu Z, et al. Histotripsy beyond the intrinsic cavitation threshold using very short ultrasound pulses: Microtripsy. IEEE Trans Ultrason Ferroelectr Freq Control. 2014;

18. Maxwell AD, Wang T-Y, Cain CA, Fowlkes JB, Sapozhnikov OA, Bailey MR, et al. Cavitation clouds created by shock scattering from bubbles during histotripsy. J Acoust Soc Am [Internet]. 2011;130(4):1888–98. Available from: http://asa.scitation.org/doi/10.1121/1.3625239

19. Coussios CC, Roy RA. Applications of Acoustics and Cavitation to Noninvasive Therapy and Drug Delivery. Annu Rev Fluid Mech. 2008 Jan;40(1):395–420.

20. Blatteau JE, Souraud JB, Gempp E, Boussuges A. Gas nuclei, their origin, and their role in bubble formation. Aviat Sp Environ Med. 2006;77(10):1068–76.

21. Davitt K, Arvengas A, Caupin F. Water at the cavitation limit: Density of the metastable liquid and size of the critical bubble. EPL. 2010;

22. Caupin F, Arvengas A, Davitt K, Azouzi MEM, Shmulovich KI, Ramboz C, et al. Exploring water and other liquids at negative pressure. J Phys Condens Matter. 2012 Jul;24(28):284110.

23. Vlaisavljevich E, Kim Y, Owens G, Roberts W, Cain C, Xu Z. Effects of tissue mechanical properties on susceptibility to histotripsy-induced tissue damage. Phys Med Biol. 2014;

24. Beegle BL, Modell M, Reid RC. Thermodynamic stability criterion for pure substances and mixtures. AIChE J. 1974;

25. DEBENEDETTI PG. Metastable Liquids [Internet]. Vol. 1. Princeton University Press; 1996. Available from: http://www.jstor.org/stable/j.ctv10crfs5

26. Herbert E, Balibar S, Caupin F. Cavitation pressure in water. Phys Rev E - Stat Nonlinear, Soft Matter Phys. 2006 Oct;74(4):41603.

27. Copelan A, Hartman J, Chehab M, Venkatesan AM. High-Intensity Focused Ultrasound: Current Status for Image-Guided Therapy. Semin Intervent Radiol [Internet]. 2015 Dec 25;32(4):398–415. Available from: http://link.springer.com/10.1134/1.1591291

28. Vehkamäki H. Classical nucleation theory in multicomponent systems. Classical Nucleation Theory in Multicomponent Systems. 2006. 1–176 p.

29. Kashchiev D. Thermodynamically consistent description of the work to form a nucleus of any size. J Chem Phys. 2003;118(4):1837–51.

30. Caupin F. Liquid-vapor interface, cavitation, and the phase diagram of water. Phys Rev E [Internet]. 2005 May 17;71(5):051605. Available from: https://link.aps.org/doi/10.1103/PhysRevE.71.051605

31. Kashchiev D. Nucleation. 1st ed. Kashchiev D, editor. Institute of Physical Chemistry, Bulgarian Academy of Sciences: Butterworth-Heinemann; 2000. (Basic Theory with Applications).

32. Blander M. Bubble nucleation in liquids. Adv Colloid Interface Sci. 1979 Sep;10(1):1–32.

33. Delale CF, Hruby J, Marsik F. Homogeneous bubble nucleation in liquids: The classical theory revisited. J Chem Phys. 2003 Jan;118(2):792–806.

34. Fisher JC. The fracture of liquids. J Appl Phys. 1948;19(11):1062–7.

35. Balibar S, Caupin F. Metastable liquids. J Phys Condens Matter. 2003 Dec;15(1):S75--S82.

36. Wagner W, Pruß A. The IAPWS formulation 1995 for the thermodynamic properties of ordinary water substance for general and scientific use. J Phys Chem Ref Data. 2002;31(2):387–535.

37. Azouzi MEM, Ramboz C, Lenain JF, Caupin F. A coherent picture of water at extreme negative pressure. Nat Phys. 2013 Jan;9(1):38–41.

38. Schmelzer JWP, Baidakov VG. Comment on "simple improvements to classical bubble nucleation models." Phys Rev E. 2016 Aug;94(2):26801.

39. Takaishi Y. New IAPWS Releases on Surface Tensions of Ordinary Water and Heavy Water Substances. Rev High Press Sci Technol No Kagaku To Gijutsu. 1997;

40. Stan CA, Willmott PR, Stone HA, Koglin JE, Liang M, Aquila AL, et al. Negative Pressures and Spallation in Water Drops Subjected to Nanosecond Shock Waves. J Phys Chem Lett. 2016;7(11).

41. Fletcher NH. Size effect in heterogeneous nucleation. J Chem Phys. 1958;

42. Briggs LJ. Limiting negative pressure of water [2]. J Appl Phys. 1950;21(7):721–2.

43. Soneson JE. A user-friendly software package for HIFU simulation. In: AIP Conference Proceedings. 2009.

44. Canney MS, Bailey MR, Crum LA, Khokhlova VA, Sapozhnikov OA. Acoustic characterization of high intensity focused ultrasound fields: A combined measurement and modeling approach. J Acoust Soc Am. 2008;

45. Pahk KJ, Gélat P, Sinden D, Dhar DK, Saffari N. Numerical and Experimental Study of Mechanisms Involved in Boiling Histotripsy. Ultrasound Med Biol [Internet]. 2017 Dec;43(12):2848–61. Available from: https://linkinghub.elsevier.com/retrieve/pii/S0301562917312991

46. Pahk KJ, de Andrade MO, Gélat P, Kim H, Saffari N. Mechanical damage induced by the appearance of rectified bubble growth in a viscoelastic medium during boiling histotripsy exposure. Ultrason Sonochem. 2019;53:164–77.

47. Pahk KJ, Dhar DK, Malago M, Saffari N. Ultrasonic histotripsy for tissue therapy. In: Journal of Physics: Conference Series. 2015.

48. Choi MJ, Guntur SR, Lee KIL, Paeng DG, Coleman A. A Tissue Mimicking Polyacrylamide Hydrogel Phantom for Visualizing Thermal Lesions Generated by High Intensity Focused Ultrasound. Ultrasound Med Biol. 2013;

49. Brennen CE. Phase Change, Nucleation, and Cavitation. In: Cavitation and Bubble Dynamics. Cambridge: Cambridge University Press; 2009. p. 1–29.

50. Katz JL, Blander M. Condensation and boiling: Corrections to homogeneous nucleation theory for nonideal gases. J Colloid Interface Sci. 1973 Jan;42(3):496–502.

51. Baidakov VG. Surface tension of cavitation pockets according to data of computer simulation of nucleation in a stretched fluid. Colloid J. 2015;77(2):119–24.

52. Maxwell AD, Cain CA, Fowlkes JB, Xu Z. Inception of cavitation clouds by scattered shockwaves. In: Proceedings - IEEE Ultrasonics Symposium. IEEE; 2010. p. 108–11.

53. Pahk KJ, Lee S, Gélat P, de Andrade MO, Saffari N. The interaction of shockwaves with a vapour bubble in boiling histotripsy: The shock scattering effect. Ultrason Sonochem. 2021;

54. Bruot N, Caupin F. Curvature-dependence of the liquid-vapor surface tension beyond the Tolman approximation. Phys Rev Lett [Internet]. 2016 Jan 4;116(5):56102. Available from: http://arxiv.org/abs/1601.00468

55. Sapozhnikov OA. High-intensity ultrasonic waves in fluids: Nonlinear propagation and effects. In: Power Ultrasonics: Applications of High-Intensity Ultrasound. 2014.

56. Khokhlova TD, Haider YA, Maxwell AD, Kreider W, Bailey MR, Khokhlova VA. Dependence of Boiling Histotripsy Treatment Efficiency on HIFU Frequency and Focal Pressure Levels. Ultrasound Med Biol. 2017;43(9):1975–85.

57. Bailey MR, Khokhlova VA, Sapozhnikov OA, Kargl SG, Crum LA. Physical mechanisms of the therapeutic effect of ultrasound (a review). Acoustical Physics. 2003.

58. Wilhelm E, Battino R, Wilcock RJ. Low-Pressure Solubility of Gases in Liquid Water. Chem Rev. 1977;77(2).

59. Gibbs JW. The collected works of J. W. Gibbs: Thermodynamics. London, Longmans, Green, & co. 1928.

60. Bader KB, Holland CK. Predicting the growth of nanoscale nuclei by histotripsy pulses. Phys Med Biol. 2016;61(7):2947–66.

61. Kreider W, Maxwell AD, Khokhlova T, Simon JC, Khokhlova VA, Sapozhnikov O, et al. Rectified growth of histotripsy bubbles. In: Proceedings of Meetings on Acoustics. 2013.

62.   Pahk KJ, Gélat P, Kim H, Saffari N. Bubble dynamics in boiling histotripsy. Ultrasound Med Biol. 2018;44(12):2673–96.